Title

Small molecule inhibitors of intestinal epithelial anion exchanger SLC26A3 (DRA) with a luminal, extracellular site of action

Permalink

https://escholarship.org/uc/item/63q5008s

Authors

Cil, Onur
Anderson, Marc O
de Souza Goncalves, Livia
et al.

Publication Date

2023-03-01

DOI

10.1016/j.ejmech.2023.115149

Peer reviewed

Small molecule inhibitors of intestinal epithelial anion exchanger SLC26A3 (DRA) with a luminal, extracellular site of action

Onur Cil[a,*,1], **Marc O. Anderson**[b,1], **Livia de Souza Goncalves**[a], **Joseph-Anthony Tan**[c], **Peter M. Haggie**[c], **Alan S. Verkman**[c]

[a]Department of Pediatrics, University of California San Francisco, San Francisco, CA, USA

[b]Department of Chemistry and Biochemistry, San Francisco State University, San Francisco, CA, USA

[c]Departments of Medicine and Physiology, University of California San Francisco, San Francisco, CA, USA

Abstract

The anion exchanger protein SLC26A3 (down-regulated in adenoma, DRA) is expressed in the luminal membrane of intestinal epithelial cells in colon, where it facilitates the absorption of Cl^- and oxalate. We previously identified a 4,8-dimethylcoumarin class of SLC26A3 inhibitors that act from the SLC26A3 cytoplasmic surface, and demonstrated their efficacy in mouse models of constipation and hyperoxaluria. Here, screening of 50,000 new compounds and 1740 chemical analogs of active compounds from the primary screen produced five novel classes of SLC26A3-selective inhibitors (1,3-dioxoisoindoline-amides; N-(5-sulfamoyl-1,3,4-thiadiazol-2-yl)acetamides; thiazolo-pyrimidin-5-ones; 3-carboxy-2-phenylbenzofurans and benzoxazin-4-ones) with IC_{50} down to 100 nM. Kinetic washout and onset of action studies revealed an extracellular site of action for the thiazolo-pyrimidin-5-one and 3-carboxy-2-phenylbenzofuran inhibitors. Molecular docking computations revealed putative binding sites for these inhibitors. In a loperamide model of constipation in mice, orally administered 7-(2-chloro-phenoxymethyl)-3-phenyl-thiazolo [3,2-a]pyrimidin-5-one (**3a**) significantly increased stool weight, pellet number and water content. SLC26A3 inhibitors with an extracellular site of action offer the possibility of creating non-absorbable, luminally acting inhibitors with minimal systemic exposure following oral administration. Our findings also suggest that inhibitors of related SLC26 anion transporters with an extracellular site of action might be identified for pharmacological modulation of selected epithelial ion transport processes.

Keywords

SLC26; Down-regulated in adenoma; Constipation; Kidney stones; Non-absorbable drugs

---

*Corresponding author. 513 Parnassus Ave, HSE-1246, San Francisco, CA, 94143, USA. onur.cil@ucsf.edu (O. Cil).
[1]These authors contributed equally to this study.

1.   Introduction

Solute carrier (SLC) proteins, which transport solutes across biological membranes, represent a large class of relatively underexplored drug targets [1]. Of the SLCs, the SLC26 family contains 11 genes encoding anion exchangers or channel-like transporters, some with broad anion specificity for chloride, bicarbonate, sulfate and oxalate [2]. These proteins are generally involved in the transport of solutes across epithelia for regulation of volume, pH and solute content in cells and bodily fluids [2,3]. Several inherited diseases are associated with loss of function mutations in these genes, including chondrodysplasias (SLC26A2) [4], chloride-losing diarrhea (SLC26A3) [5,6] and Pendred syndrome (SLC26A4) [7].

SLC26A3 (down-regulated in adenoma, DRA) is of particular interest as a drug target because of its involvement in intestinal absorption of chloride and oxalate [3,8]. SLC26A3 is expressed mainly in epithelial cells lining the colon, and to a lesser extent in small intestine and some tissues outside of the intestine including prostate [9–11]. Mice lacking SLC26A3 manifest diarrhea [5] and reduced urinary oxalate [12], which is also seen in humans with loss of function mutations in SLC26A3 [13]. Inhibition of SLC26A3-mediated Cl^- and oxalate absorption may thus have therapeutic utility in various forms of constipation as well as hyperoxaluria, a major risk factor for calcium oxalate kidney stones.

Using a cell-based high-throughput screen, we previously identified a 4,8-dimethylcoumarin class of compounds that inhibited SLC26A3-mediated anion exchange with IC_{50} down to 25 nM, which were selective for SLC26A3 when tested against related SLC26 family members and other major epithelial ion transporters. Kinetic studies revealed an intracellular (cytoplasmic) site of action of the 4,8-dimethylcoumarins [14,15]. A lead candidate, [7-(3-iodobenzyloxy)-4,8-dimethylcoumarin]-3-acetic acid (DRA_{inh}-A270), was effective in improving stool output and hydration in a mouse model of constipation produced by loperamide [15], and in preventing hyperoxaluria and oxalate nephropathy in mice orally loaded with oxalate [16]. In closed colonic loops in mice, DRA_{inh}-A270 inhibited the absorption of fluid and oxalate from the loop lumen [16], supporting a mechanism of action involving direct inhibition of chloride and oxalate absorption.

The goal of this study was to identify small molecule SLC26A3 inhibitors with an extracellular site of action, which affords the unique opportunity for creation of non-absorbable, luminally acting inhibitors with minimal systemic exposure. Although high-resolution crystal structures of SLC26A3 or its closest homologs have not been solved, homology modeling based on the structure of the murine SLC26A9 protein indicates substantial extracellular exposure and hence the possibility of identifying extracellularly acting inhibitors [17]. We report here the discovery and structure-activity relationship studies of five novel chemical classes of SLC26A3-selective inhibitors, two of which have an extracellular site of action. In vivo testing of a thiazolo-pyrimidin-5-one inhibitor in mice showed efficacy in a loperamide-induced model of constipation.

2.   Methods

2.1.   Compounds

Primary high-throughput screening was done using a collection of 50,000 chemically diverse, drug-like, synthetic small molecules not previously tested (ChemDiv, San Diego, CA). Initial screening was done at a concentration of 25 μM. Following prioritization and selection of five chemical classes of active compounds, SLC26A3 transport assays were done on 1740 commercially available (ChemDiv) structural analogs of active compounds. Commercial analogs were selected by holding the core scaffold constant and allowing variation of substituents on attached ring systems, typically substituted phenyl groups.

2.2.   Cell culture and transport assays

Fischer rat thyroid (FRT) cells stably expressing murine slc26a3 and a halide sensing (with mutations H148Q/I152L/F46L) yellow fluorescent protein (FRT-YFP-slc26a3 cells) were generated and cultured as described [14,18]. For assay of iodide-chloride exchange, cells cultured on 96-well plates were incubated in phosphate buffered saline (PBS) prior to addition of iodide-substituted PBS (NaCl replaced with 140 mM NaI), as described [18]. The rate of fluorescence quenching following iodide addition, determined by mono-exponential regression, provided a quantitative measure of chloride/iodide exchange. IC_{50} values were determined from assays done at different inhibitor concentrations using a single-site inhibition model. Selectivity studies were done using YFP-based assays of SLC26A4, slc26a6, slc26a9, CFTR and TMEM16A, as described [14].

2.3.   Screening

High-throughput screening to identify SLC26A3 inhibitors was done on FRT-YFP-slc26a3 cells using a semi-automated Beckman Coulter (Indianapolis, IN) platform with FLUOstar OMEGA plate readers (BMG Labtech, Cary, NC), as described [14,18]. Cells were plated in 96-well black-walled, clear-bottom tissue culture plates (Corning Life Sciences, Tewksbury, MA) at a density of 20,000 cells/well and used after 48 h when confluent. Assays were done in each well by continuous measurement of YFP fluorescence for 1 s before and 12 s after addition of an iodide-containing solution using an automated syringe pump. All plates contained negative (1% DMSO) and positive (5 μM DRA_{inh}-A270) controls.

2.4.   Kinetic studies of inhibitor action

The time course of onset of inhibitor action was measured using the YFP plate reader assay in which inhibitors (at concentration approximately 2 x IC_{50}) were added at specified times prior to assay. For washout studies, cells were incubated with inhibitors (at concentration approximately 5 x IC_{50}) for 10 min, washed rapidly with PBS containing 1% bovine serum albumin, and then incubated for specified times with 100 μL PBS prior to YFP plate reader assay. Parallel studies were done without inhibitor washout for comparison.

2.5. Animals

Animal experiments were approved by the UCSF Institutional Animal Care and Use Committee (IACUC). CD1 mice were bred in house and used for experiments at 8–12 weeks of age.

2.6. Murine model of constipation

Constipation was induced in CD1 mice by administration of loperamide (0.3 mg/kg, intraperitoneal) in PBS containing 5% ethanol (or vehicle control), as described [19,20]. Test compounds were administered by oral gavage at 10 mg/kg in saline containing 5% DMSO and 10% Kolliphor-HS (or vehicle without compound) 1 h before loperamide. After loperamide injection, mice were placed in metabolic cages with free access to food and water for collection of stool samples over 3 h. Total stool weight and number of fecal pellets were measured, and stool water content was determined from wet and dry stool weights, as described [19,20].

2.7. Homology modeling and docking computations

A homology model of human SLC26A3 (accession code NP_000102.1) was generated using molecular modeling software (YASARA, v. 19.12.14; Vienna, Austria) in automated mode [21]. The model used coordinates from a recently solved 3.96 Å resolution cryo-EM structure of the homologous anion channel protein, mouse SLC26A9 (PDB, 6RTC) as a homology template [17]. The homology model was prepared for docking using the FRED-RECEPTOR utility (OpenEye Scientific Software, Santa Fe, NM), with cytoplasmic and extracellular domains defined with 10 cubic Å boxes. Structures of the inhibitor molecules were converted to SMILES strings, transformed to three-dimensional conformations, and minimized using PIPELINE PILOT (Accelrys, San Diego, CA). Single conformations were passed through MOLCHARGE (OpenEye) to apply MMFF charges and through OMEGA (OpenEye) to generate multi-conformational libraries, which were docked using FRED (OpenEye). Bound complexes were visualized using PyMOL (Schrödinger, LLC, San Diego, CA).

2.8. Statistics

Student's t-test (two-tailed) was used for statistical analysis and $P < 0.05$ was considered statistically significant.

3. Results

3.1. Inhibitor discovery by high-throughput screening

Primary screening was carried out on a chemically diverse collection of 50,000 drug-like synthetic small molecules that were not tested previously. As described before [14], the assay utilized FRT epithelial cells stably co-expressing murine slc26a3 and a cytoplasmic YFP halide sensor. Iodide influx into cells was quantified from the kinetics of fluorescence quenching following iodide addition to the extracellular solution overlying cells in a 96-well plate format. Cells were incubated with test compounds at 25 μM for approximately 10 min prior to transport assays. Primary screening yielded compounds from five novel chemical

classes that produced >75% inhibition of slc26a3-mediated iodide influx, in addition to compounds related to previously identified inhibitors. Fig. 1 provides the core chemical structures of each novel inhibitor class.

3.2. Structure-activity relationship studies

SLC26A3 function was assayed on 1740 commercially available analogs of the five chemical classes of inhibitors. Table-1 lists IC_{50} values for the most potent compounds of each class, with concentration-inhibition measurements for the most potent inhibitor of each class shown in Fig. 2. The structural determinants for SLC26A3 inhibition by each of the five compound classes are summarized diagrammatically in Figs. S1–S5 (Supplementary Information).

The 1,3-dioxoisoindoline (phalthalimide) core scaffold contains a N-substitution and a carboxamide substituent at the 4-position. The best substituents at the R^1 position (N2) were 4-chlorophenyl (**1a**) and 3,4-dimethylphenyl (**1b**). Replacement of this substituent with linear or branched alkyl system (C_3 or C_5) (**1c**, **1e**, **1n**) reduced or eliminated inhibition potency. Other substituted aryl rings (**1d**, **1f-1g**, **1j-1m**) or 2-methyltetrafuran (**1h**) reduced potency. At the R^2 position (C5), phenyl-2-carboxylic acid linked via an amide was the best, with additional aryl substitution giving reduced inhibition potency.

The second compound class contains a thiadiazole central scaffold with an N-disubstituted sulfonamide (R^1 and R^2) at the C2 position and an aminoacyl linked group (R^3) extending from C5. Several variations of substituents attached to this scaffold were active. In the first variation, represented by the most potent inhibitor (**2a**), at R^1 was 3,5-dimethylphenyl, at R^2 was methyl, and at R^3 was 3,4-dimethylphenoxy-methylene. Two slightly less potent compounds (**2b** and **2c**) had 3-methyl-phenyl at position R^1, no substitution at R^2, and either 2-methylphenyl or 3-methoxyphenyl at R^3. In another less potent variation (**2d**), R^1 and R^2 were substituted with indolin-1-yl, while R^3 contained 4-methylphenoxy methylene.

The third compound class contains a thiazolo-pyrimidin-5-one heterocycle with tethered ring systems at R^1, phenyl at R^2, and hydrogen at R^3. Only variations of groups tethered to R^1 were explored because of limited commercially available analogs. The most potent compounds were attached via an ether linkage to 2-chlorophenoxy-methylene (**3a**) or 2-chlorobenzyl-thiomethylene (**3b**). Analogs of **3a** that incorporate a 2,4-dichlorophenoxy ring system (**3c**) or a 2-methylbenzoate ester-linkage (**3d**) had reduced potency.

The fourth compound class consists of 3-carboxy-2-phenylbenzofurans. At R^1, the best substituent was phenyl (**4a-4g**), with R^1 as methyl having reduced potency (**4h**). At R^2, carboxylic acid was the best, while methyl esters (e.g. **4h**) had reduced potency and other esters were inactive. The R^3 position was explored most extensively, with benzyloxy groups generally having the best potency, particularly with substituents including 2-methyl (**4a**) and 2-chloro (**4b**). Other simple substitutions of methyl-and chloro-benzyl at R^3 were less potent (**4c-4f**), as well as unsubstituted benzyl (**4g**). Benzyl substituents at the ortho position may be favored (**4a** and **4b**). Various other oxygen-linked groups on the benzyloxy ring system at R^3 were found to be inactive (substituted acyl, ethers, ethers linked to esters or ketones).

The final compound class contains a benzoxazin-4-one heterocycle core. The most potent inhibitors were unsubstituted at R^2, R^3, and R^4, while methyl at these positions was tolerated but with loss of potency. At R^1, phenyl linked at the 3-position to the nitrogen of substituted benzamides, e.g. 4-chloro (**5a**), 4-ethoxy (**5b**), 2-bromo (**5c**), had the best potency. At R^1, compounds with phenyl linked at the 3-position via nitrogen to substituted phenoxyacetyl (**5d** and **5e**) groups had reduced potency. Compounds with the 3-aminobenzene linkage connected to *N*-acetamide (**5f**), *N*-pivalamide (**5g**), and *N*-isobutyramide (**5h**) had slightly reduced potency.

3.3.   Synthesis of thiazolo-pyrimidin-5-one (3a) and 3-carboxy-2-phenylbenzofuran (4a)

The lead compounds in the thiazolo-pyrimidin-5-one (**3a**) and 3-carboxy-2-phenylbenzofuran (**4a**) scaffolds were resynthesized in >95% pure form (determined by HPLC and NMR analysis) to verify the structures and to provide material for further characterization (Scheme 1). For **3a**, 2-amino-4-phenylthiazole (**6**) was reacted with ethyl 4-chloroacetoacetate (**7**) in the presence of polyphosphoric acid to cause a cyclo-condensation sequence to generate the key thiazolo-pyrimidin-5-one building block (**8**). This key intermediate was reacted with 2-chlorophenol in the presence of Cs_2CO_3 and NaI, employing Finkelstein conditions to generate the ether linkage to give the final thiazolo-pyrimidin-5-one inhibitor **3a**. For 3-carboxy-2-phenylbenzofuran inhibitors, commercially available 5-hydroxy-2-phenyl-benzofuran-3-carboxylic acid ethyl ester (**9**) was alkylated in the presence of Cs_2CO_3 with substituted benzyl bromides to generate benzyl ether intermediates **11a**-**c**. A practical issue in the benzylation is similar polarity of the product with the benzyl bromide starting materials. We found that by adding 3,4-dihydroxybenzoic acid (**10**) after the benzylation, that excess benzyl bromide can be scavenged and more readily separated by chromatography. The ester functionalities in these molecules were easily hydrolyzed using KOH to yield the carboxylic acid-containing products **4a**-**4c**. By employing the scavenger strategy, the final products were highly pure and did not require additional purification.

A proposed mechanism of the cyclo-condensation of 2-amino-4-phenylthiazole (**6**) with ethyl 4-chloroacetoacetate (**7**) to form building block **8** is presented in Fig. 3. We envision that the more nucleophilic primary amine of thiazole **6** reacts with the electrophilic ketone functionality of **7**, initially, to create an imine intermediate **12**. Thereafter, accompanied by proton transfer steps, the thiazole nitrogen atom in **12** attacks the ethyl ester, to form the desired thiazolo-pyrimidin-5-one heterocycle **8**. The remaining mechanisms to generate **3a** and **4a**-**4c** occur through base-mediated alkylation and ester hydrolysis.

3.4.   Inhibitor selectivity

Selectivity studies were carried out for the most potent SLC26A3 inhibitors of each of the five chemical classes. Inhibition assays were done on a panel of SLC26-family homologs (SLC26A4, SLC26A6, SLC26A9), as well as CFTR and TMEM16A, two major epithelial chloride channels that are expressed in intestine (Table-2). The compounds generally had very good selectivity at a high concentration of 10 μM in which SLC26A3 was inhibited by >90%, except for **2a** which produced >80% inhibition of TMEM16A.

3.5. Inhibitor site of action

Inhibitor site of action was investigated from the kinetics of inhibition following addition to the extracellular solution and the kinetics of loss of inhibition after washout. In preliminary studies, inhibitors were added at a concentration of 2-fold their IC_{50} and SLC26A3 inhibition was assessed at 14 s, the earliest technically feasible time point after inhibitor addition. Compounds **3a** and **4a** produced $66 \pm 7\%$ and $38 \pm 8\%$ maximal inhibition, respectively at 14 s, whereas the dimethycoumarin DRA_{inh}-A270 had a slow onset of action with $8 \pm 2\%$ maximal inhibition at 14 s and $86 \pm 3\%$ inhibition at 10 min. As a more definitive assessment of site of action, cells were first incubated for 10 min with inhibitors at a concentration of 5-fold their IC_{50} in order to load cytoplasm with inhibitors in their free and bound states (Fig. 4). Following rapid washout, inhibitors with a cytoplasmic site of action would be reversed minimally, whereas inhibitors with an extracellular site of action could be reversed rapidly as cellular efflux is not required. Compound **3a** produced $92 \pm 1.9\%$ inhibition following 10 min incubation, which was reduced to $32 \pm 1.4\%$ just after washout. Compound **4a** produced $87 \pm 1.4\%$ inhibition following 10 min incubation, which was reduced to $25 \pm 0.9\%$ just after washout. In contrast, the previously identified inhibitor with presumed intracellular site of action, DRA_{inh}-A270, produced $100 \pm 0.4\%$ inhibition effect following 10 min incubation, which was not significantly reduced ($98 \pm 1\%$ inhibition) just after washout.

3.6. Molecular modeling reveals a potential binding site of externally acting DRA inhibitors

A homology model of human SLC26A3 was created using as template a cryo-EM structure of the homologous transporter mouse SLC26A9 (PDB, 6RTC), with potential inhibitor binding sites identified using an automated receptor identification tool (see Methods). Compounds **3a** and **4a** were docked to an extracellular binding site on SLC26A3 (Fig. 5). A zoomed-in view of docked **4a** shows potential hydrophobic interactions of the core heterocycle with Leu^{169}, Leu^{168}, Pro^{101}, Asp^{99}, and phe^{228}. Lys^{137} is positioned to make a hydrogen bond with the C2-carboxylate of the inhibitor scaffold. Other residues on the periphery of the substituted phenyl are Thr^{223}, Val^{224}, and Ser^{236}, though the distance of these residues from the inhibitor suggests tolerance for additional substitutions on the phenyl ring. The docked structure of **3a** is also shown, which has unsubstituted and substituted phenyl groups that are similarly oriented in the putative binding site. For comparison, the cytoplasmic acting inhibitor DRA_{inh}-A270 is shown in a putative binding site on the cytoplasmic surface of the SLC26A3 homology model.

3.7. Efficacy of 3a in a loperamide-induced mouse model of constipation

Orally administered **3a** at 10 mg/kg was tested in a loperamide-induced model of constipation in mice. Loperamide resulted in marked constipation with >90% reduced stool weight and pellet number compared to control mice (Fig. 6). Compound **3a** significantly increased stool weight and number of pellets, albeit modestly. However, because loperamide affects intestinal motility, stool weight and pellet number are imperfect outcome measures for testing ion transport modulators. Stool hydration as quantified by water content, which is a superior outcome measure used in constipation models [19,20,22], was significantly

increased by **3a** in loperamide-treated mice from $49 \pm 2\%$ (in vehicle control) to $55 \pm 2\%$, demonstrating its efficacy in increasing stool hydration.

4. Discussion

Small molecule screening produced five distinct chemical classes of SLC26A3 inhibitors that differed structurally from inhibitors identified in our initial screen [14,15]. Each of the scaffolds had evolvable SAR characteristics with distinct structural determinants for SLC26A3 inhibition. The best compounds of each class had IC_{50} values in the nanomolar range and were generally selective for SLC26A3 when tested at 10 μM against related members of the SLC26 family and the epithelial chloride channels CFTR and TMEM16A. Having multiple different chemical scaffolds is advantageous should lead candidates fail in later stages of preclinical or clinical testing. Of greatest interest herein was the finding that the thiazolo-pyrimidin-5-one and 3-carboxy-2-phenyl-benzofuran inhibitors had an apparent extracellular site of action, as evidenced by their rapid kinetics of inhibition onset and washout, and improvement of stool output and hydration with oral administration in a loperamide model of constipation. Considering that SLC26A3 is expressed in the lumen-facing membrane of intestinal epithelial cells, the inhibitors with extracellular site of action offer the opportunity of developing luminally active, non-absorbable drug candidates.

There are significant potential advantages of non-absorbable drugs acting on epithelial cells in the gastrointestinal tract as compared to drugs that are absorbed into the systemic circulation and delivered to their target through the bloodstream [23]. An orally administered non-absorbable drug with little systemic exposure minimizes off-target effects outside of the intestine, reducing potential drug toxicity and allowing higher dosage for greater effect on the lumen-facing intestinal target [23]. For example, the approved drug tenapanor is a poorly absorbed inhibitor of the sodium-proton exchanger NHE3 that is expressed in the luminal membrane of epithelial cells in small intestine as well as in many cell types outside of the intestine [24]. Tenapanor is a relatively large, 1145 Da compound consisting of two inhibitory small molecules joined by a polar linker [25]. Another example, developed by our lab, are luminally active, non-absorbable CFTR inhibitors for anti-secretory therapy of cholera and other CFTR-mediated secretory diarrheas [26,27]. The inhibitors consist of macromolecular conjugates of an extracellularly acting malonic acid hydrazide CFTR inhibitor discovered in a small molecule screen. The externally acting SLC26A3 inhibitors identified here are the first, to our knowledge, SLC26 modulators with an extracellular site of action. It follows that externally acting inhibitors may be identified for other SLC26 proteins, such as SLC26A6 (PAT1), the luminal anion exchanger in small intestine [18], and SLC26A4 (pendrin), a luminal anion exchanger in inflamed airways [28].

To identify potential inhibitor binding sites on the SLC26A3 protein, the externally acting inhibitors **3a** and **4a**, and the internally acting inhibitor DRA_{inh}-A270, were docked to a homology model of SLC26A3 that was created based on a cryo EM structure of mouse SLC26A9 [17]. A surface of non-polar residues around the 3-carboxy-2-phenylbenzofuran scaffold was seen in which the binding model predicted a potentially important interaction between the inhibitor carboxylate group and Lys[137]. Notably, 2-phenylbenzofuran analogs with this key carboxylate replaced with esters, ethers, or a farther linked carboxylate

were less potent or inactive. That some analogous benzofuran inhibitors are active against SLC26A3 and SLC26A4 is interesting (e.g. **4h**, where R^1 = methyl), and could suggest a similar mode of binding for these targets. The proposed binding model for the thiazolo-pyrimidin-5-ones (e.g. **3a**) is similar to that for the 3-carboxy-2-phenylbenzofurans (e.g. **4a**). For example, the methylene 2-chlorophenoxy ring system in **3a** is situated in the binding pocket area, similar to the 2-methylbenzyloxy group in **4a**, and a similar position was found for the un-substituted phenyl rings. Notably, the models predict space around the un-substituted phenyls in **3a** and **4a** (near Pro^{101} and Gly^{319}), which inspired a strategy we are currently undertaking to incorporate substituents on these rings through synthesis.

The SAR and docking results for the two classes of SLC26A3 inhibitors with an extracellular site of action suggest approaches for synthesis of a non-absorbable macromolecular conjugate of an active inhibitor with a water-soluble macromolecule such as methyl-terminated polyethylene glycol (mPEG). For example, mPEG might be attached to the substituted R^3 benzyloxy in 3-carboxy-2-phenyl benzofurans (**4**), or to the R^1 methylene phenoxy of thiazolo-pyrimidin-5-ones (**3**). We envision a conjugate with attachment from the phenyl 2- or 3-positions that would not interfere with binding to SLC26A3 while allowing the mPEG to project away from the protein surface. Further, we envision synthesis of dually-linked bis-PEG conjugates based on **3** or **4**, analogous to the NHE3 inhibitor tenapanor [29].

There are a few literature reports on the biological activity of the 3-carboxy-2-phenylbenzofuran (**4**) and thiopyrimidin-5-one (**3**) scaffolds. For the 3-carboxy-2-phenylbenzofuran scaffold, our laboratory previously reported inhibitors with the same general structure but with R^1 as 4-methylphenyl, 4-methoxyphenyl, or naphthyl rather than phenyl [30]. The best compound in this series had an IC_{50} of 2.8 μM for chloride channel inhibition, much higher than the IC_{50} of 340 nM for SLC26A3 inhibition by **4a**. A less substituted benzofuran scaffold (with R^1 = H) has been reported to be active against gherlin O-acyltransferase, a drug target for obesity [31,32]. Another analogous benzofuran scaffold (R^3 = vinyl carboxylic acid) was found to inhibit lipid peroxidation [33]. The synthesis and reactivity of benzofurans has been reviewed extensively, and continues to be an active research pursuit [34–36]. Furocoumarins, that contain the benzofuran heterocycle, have been reviewed in terms of their synthetic preparation and use as a photo-therapy for the skin disorders such as psoriasis and vitiligo [37]. For the thiopyrimidin-5-one scaffold (**3**), there are no reports of compounds with closely similar structure to the compound reported here containing R^1 substituted methylene phenoxy (**3a**) or methyl thiobenzyl (**3b**). Analogs in which R^1 is replaced with NH-aryl were reported with antibacterial and antitubercular activity [38]. Another set of analogs where R^1 contains methylene phenoxy (like **3a**), but with N-methyl carboxamide at R^3, were found to modulate NMDA function for potential antipsychotic activity [39,40]. Less similar analogs of the thiopyrimidin-5-one scaffold, where C6 position is tethered to a 6-fluorobenzisoxazole, have been reported with antipsychotic activity [41]. Another set of more distant analogs to scaffold **3**, namely thiazolopyrimidines, were shown to have antioxidant and antitumor activity [42]. Among the additional inhibitor scaffolds explored in this study, thiadiazoles (a heterocycle present in

inhibitor class **2**) have been shown to have anti-microbial activity and cytotoxicity against some human cancer cell lines [43–46].

The major indications for pharmacological inhibition of SLC26A3 in intestine include constipation and conditions associated with high urinary oxalate including enteric hyperoxaluria and calcium oxalate nephrolithiasis. Each of these indications is common and presents an unmet need, as approved drugs for constipation have limited efficacy [47] and there are no approved drugs for treatment of enteric hyperoxaluria. Inhibition of intestinal chloride and fluid absorption is predicted to be beneficial for all major types of constipation, including chronic idiopathic constipation, opioid-induced constipation, and constipation-predominant irritable bowel syndrome. SLC26A3 inhibition would be uniquely suited for cystic fibrosis-associated constipation in which CFTR chloride secretion is defective and the approved drugs linaclotide, plecanatide and lubiprostone require functional CFTR for their action [48]. Inhibition of colonic oxalate absorption is predicted to be beneficial for enteric hyperoxaluria associated with a variety of conditions including bariatric surgery, pancreatic insufficiency, inflammatory bowel disease, and intestinal resection. Notwithstanding its rapid washout kinetics, a luminally acting SLC26A3 inhibitor is potentially suitable for treatment of each of these conditions.

In conclusion, we discovered and characterized SLC26A3 inhibitors with a luminal site of action. These compounds can form the basis of developing non-absorbable drug candidates with minimal systemic side effects for treatment of constipation and hyperoxaluria.

Supplementary Material

Refer to Web version on PubMed Central for supplementary material.

Acknowledgments

Declaration of competing interest

The authors declare the following financial interests/personal relationships which may be considered as potential competing interests: Onur Cil reports financial support was provided by National Institute of Diabetes and Digestive and Kidney Diseases. Onur Cil reports a relationship with Cystic Fibrosis Foundation that includes: funding grants. Onur Cil, Peter M. Haggie, Alan S. Verkman has patent pending to UCSF.

Data availability

Data will be made available on request.

Abbreviations:

SLC	Solute carrier
DRA	down-regulated in adenoma

FRT	Fischer rat thyroid
PBS	phosphate buffered saline
YFP	yellow fluorescent protein
mPEG	methyl-terminated polyethylene glycol

References

[1]. Lin L, et al. , SLC transporters as therapeutic targets: emerging opportunities, Nat. Rev. Drug Discov 14 (8) (2015) 543–560. [PubMed: 26111766]

[2]. Alper SL, Sharma AK, The SLC26 gene family of anion transporters and channels, Mol. Aspect. Med 34 (2–3) (2013) 494–515.

[3]. Dorwart MR, et al. , The solute carrier 26 family of proteins in epithelial ion transport, Physiology 23 (2008) 104–114. [PubMed: 18400693]

[4]. Forlino A, et al. , A diastrophic dysplasia sulfate transporter (SLC26A2) mutant mouse: morphological and biochemical characterization of the resulting chondrodysplasia phenotype, Hum. Mol. Genet 14 (6) (2005) 859–871. [PubMed: 15703192]

[5]. Schweinfest CW, et al. , slc26a3 (dra)-deficient mice display chloride-losing diarrhea, enhanced colonic proliferation, and distinct up-regulation of ion transporters in the colon, J. Biol. Chem 281 (49) (2006) 37962–37971. [PubMed: 17001077]

[6]. Hoglund P, et al. , Mutations of the Down-regulated in adenoma (DRA) gene cause congenital chloride diarrhoea, Nat. Genet 14 (3) (1996) 316–319. [PubMed: 8896562]

[7]. Everett LA, et al. , Pendred syndrome is caused by mutations in a putative sulphate transporter gene (PDS), Nat. Genet 17 (4) (1997) 411–422. [PubMed: 9398842]

[8]. Shcheynikov N, et al. , Coupling modes and stoichiometry of Cl-/HCO3- exchange by slc26a3 and slc26a6, J. Gen. Physiol 127 (5) (2006) 511–524. [PubMed: 16606687]

[9]. Schweinfest CW, et al. , Identification of a colon mucosa gene that is down-regulated in colon adenomas and adenocarcinomas, Proc. Natl. Acad. Sci. U. S. A 90 (9) (1993) 4166–4170. [PubMed: 7683425]

[10]. Walker NM, et al. , Down-regulated in adenoma Cl/HCO3 exchanger couples with Na/H exchanger 3 for NaCl absorption in murine small intestine, Gastroenterology 135 (5) (2008) 1645–1653 e3. [PubMed: 18930060]

[11]. Byeon MK, et al. , The down-regulated in adenoma (DRA) gene encodes an intestine-specific membrane glycoprotein, Oncogene 12 (2) (1996) 387–396. [PubMed: 8570216]

[12]. Freel RW, Whittamore JM, Hatch M, Transcellular oxalate and Cl- absorption in mouse intestine is mediated by the DRA anion exchanger Slc26a3, and DRA deletion decreases urinary oxalate, Am. J. Physiol. Gastrointest. Liver Physiol 305 (7) (2013) G520–G527. [PubMed: 23886857]

[13]. Wedenoja S, et al. , The impact of sodium chloride and volume depletion in the chronic kidney disease of congenital chloride diarrhea, Kidney Int. 74 (8) (2008) 1085–1093. [PubMed: 18827800]

[14]. Haggie PM, et al. , SLC26A3 inhibitor identified in small molecule screen blocks colonic fluid absorption and reduces constipation, JCI Insight 3 (14) (2018), e121370. [PubMed: 30046015]

[15]. Lee S, et al. , 4,8-Dimethylcoumarin inhibitors of intestinal anion exchanger slc26a3 (downregulated in adenoma) for anti-absorptive therapy of constipation, J. Med. Chem 62 (17) (2019) 8330–8337. [PubMed: 31389695]

[16]. Cil O, et al. , Small-molecule inhibitor of intestinal anion exchanger SLC26A3 for treatment of hyperoxaluria and nephrolithiasis, JCI Insight 7 (13) (2022), e153359. [PubMed: 35608921]

[17]. Walter JD, Sawicka M, Dutzler R, Cryo-EM structures and functional characterization of murine Slc26a9 reveal mechanism of uncoupled chloride transport, Elife 24 (8) (2019), e46986.

[18]. Cil O, et al. , SLC26A6-selective inhibitor identified in a small-molecule screen blocks fluid absorption in small intestine, JCI Insight 6 (11) (2021), e147699. [PubMed: 34100381]

[19]. Cil O, et al. , CFTR activator increases intestinal fluid secretion and normalizes stool output in a mouse model of constipation, Cell. Mol. Gastroenterol. Hepatol 2 (3) (2016) 317–327. [PubMed: 27127798]

[20]. Cil O, et al. , Phenylquinoxalinone CFTR activator as potential prosecretory therapy for constipation, Transl. Res 182 (2017) 14–26 e4. [PubMed: 27815136]

[21]. Land H, Humble MS, YASARA: a tool to obtain structural guidance in biocatalytic investigations, Methods Mol. Biol 1685 (2018) 43–67. [PubMed: 29086303]

[22]. Narita Y, et al. , Comparative study of constipation exacerbation by potassium binders using a loperamide-induced constipation model, Int. J. Mol. Sci 21 (7) (2020) 2491. [PubMed: 32260183]

[23]. Charmot D, Non-systemic drugs: a critical review, Curr. Pharmaceut. Des 18 (10) (2012) 1434–1445.

[24]. Mousavi T, Nikfar S, Abdollahi M, An update on efficacy and safety considerations for the latest drugs used to treat irritable bowel syndrome, Expet Opin. Drug Metabol. Toxicol 16 (7) (2020) 583–604.

[25]. Rosenbaum DP, Yan A, Jacobs JW, Pharmacodynamics, safety, and tolerability of the NHE3 inhibitor tenapanor: two trials in healthy volunteers, Clin. Drug Invest 38 (4) (2018) 341–351.

[26]. Sonawane ND, et al. , Lectin conjugates as potent, nonabsorbable CFTR inhibitors for reducing intestinal fluid secretion in cholera, Gastroenterology 132 (4) (2007) 1234–1244. [PubMed: 17408659]

[27]. Sonawane ND, et al. , Nanomolar CFTR inhibition by pore-occluding divalent polyethylene glycol-malonic acid hydrazides, Chem. Biol 15 (7) (2008) 718–728. [PubMed: 18635008]

[28]. Haggie PM, et al. , Inhibitors of pendrin anion exchange identified in a small molecule screen increase airway surface liquid volume in cystic fibrosis, Faseb. J 30 (6) (2016) 2187–2197. [PubMed: 26932931]

[29]. Labonte ED, et al. , Gastrointestinal inhibition of sodium-hydrogen exchanger 3 reduces phosphorus absorption and protects against vascular calcification in CKD, J. Am. Soc. Nephrol 26 (5) (2015) 1138–1149. [PubMed: 25404658]

[30]. Kumar S, et al. , Novel 5-substituted benzyloxy-2-arylbenzofuran-3-carboxylic acids as calcium activated chloride channel inhibitors, Bioorg. Med. Chem 20 (14) (2012) 4237–4244. [PubMed: 22739085]

[31]. Takakura N, et al., Aromatic Ring Compound. August 29, 2013 (PCT/JP2013055605 - WO 2013/125732A1).

[32]. Moose JE, et al. , An overview of ghrelin O-acyltransferase inhibitors: a literature and patent review for 2010-2019, Expert Opin. Ther. Pat 30 (8) (2020) 581–593. [PubMed: 32564644]

[33]. Maeda S, Masuda H, Tokoroyama T, Studies on the preparation of bioactive lignans of oxidative coupling reaction. I. Preparation and lipid peroxidation inhibitory effect of benzofuran lignans related to schizotenuins, Chem. Pharm. Bull (Tokyo) 42 (12) (1994) 2500–2505.

[34]. Chiummiento L, et al. , Last decade of unconventional methodologies for the synthesis of substituted benzofurans, Molecules 25 (10) (2020).

[35]. Abu-Hashem AA, et al. , Synthesis of benzofuran derivatives via different methods, Synth. Commun 44 (16) (2014) 2285–2312.

[36]. Abu-Hashem AA, et al. , Reactivity of benzofuran derivatives, Synth. Commun 44 (20) (2014) 2899–2920.

[37]. Abu-Hashem AA, El-Shazly M, Synthesis, reactions and biological activities of furochromones: a review, Eur. J. Med. Chem 90 (2015) 633–665. [PubMed: 25499986]

[38]. Cai D, et al. , Synthesis of some new thiazolo[3,2-a]pyrimidine derivatives and screening of their in vitro antibacterial and antitubercular activities, Med. Chem. Res 25 (2) (2016) 292–302.

[39]. Yu J, et al., Thiazolopyrimidinones as Modulators of NMDA Receptor Activity. April 16, 2015 (PCT/EP2014/071522 - WO 2015/052226A1).

[40]. Santangelo RM, et al. , Novel NMDA receptor modulators: an update, Expert Opin. Ther. Pat 22 (11) (2012) 1337–1352. [PubMed: 23009122]

[41]. Foguet R, et al., 5H-Thiazolo[3,2-a]pyrimidin-5-one derivatives, 1996 (PTC/EP96/02254 - WO 96/37498A1).

[42]. Abu-Hashem AA, Youssef MM, Hussein HAR, Synthesis, antioxidant, antituomer activities of some new thiazolopyrimidines, pyrrolothiazolopyrimidines and triazolopyrrolothiazolopyrimidines derivatives, J. Chin. Chem. Soc 58 (1) (2011) 41–48.

[43]. Atmaram UA, Roopan SM, Biological activity of oxadiazole and thiadiazole derivatives, Appl. Microbiol. Biotechnol 106 (9–10) (2022) 3489–3505. [PubMed: 35562490]

[44]. Abu-Hashem AA, Al-Hussain SA, Design, synthesis of new 1,2,4-triazole/1,3,4-thiadiazole with spiroindoline, imidazo[4,5-b]quinoxaline and thieno[2,3-d] pyrimidine from isatin derivatives as anticancer agents, Molecules 27 (3) (2022).

[45]. Gouda MA, et al. , Recent progress on coumarin scaffold-based anti microbial agents (Part III), J. Heterocycl. Chem 57 (11) (2020) 3784–3817.

[46]. Abu-Hashem AA, Faty AMR, Synthesis, antimicrobial evaluation of some new 1, 3, 4-thiadiazoles and 1, 3, 4- thiadiazines, Curr. Org. Synth 15 (8) (2018) 1161–1170.

[47]. Bharucha AE, Wouters MM, Tack J, Existing and emerging therapies for managing constipation and diarrhea, Curr. Opin. Pharmacol 37 (2017) 158–166. [PubMed: 29172123]

[48]. Oak AA, et al. , Lubiprostone is non-selective activator of cAMP-gated ion channels and Clc-2 has a minor role in its prosecretory effect in intestinal epithelial cells, Mol. Pharmacol 102 (2) (2022) 106–115. [PubMed: 35680165]
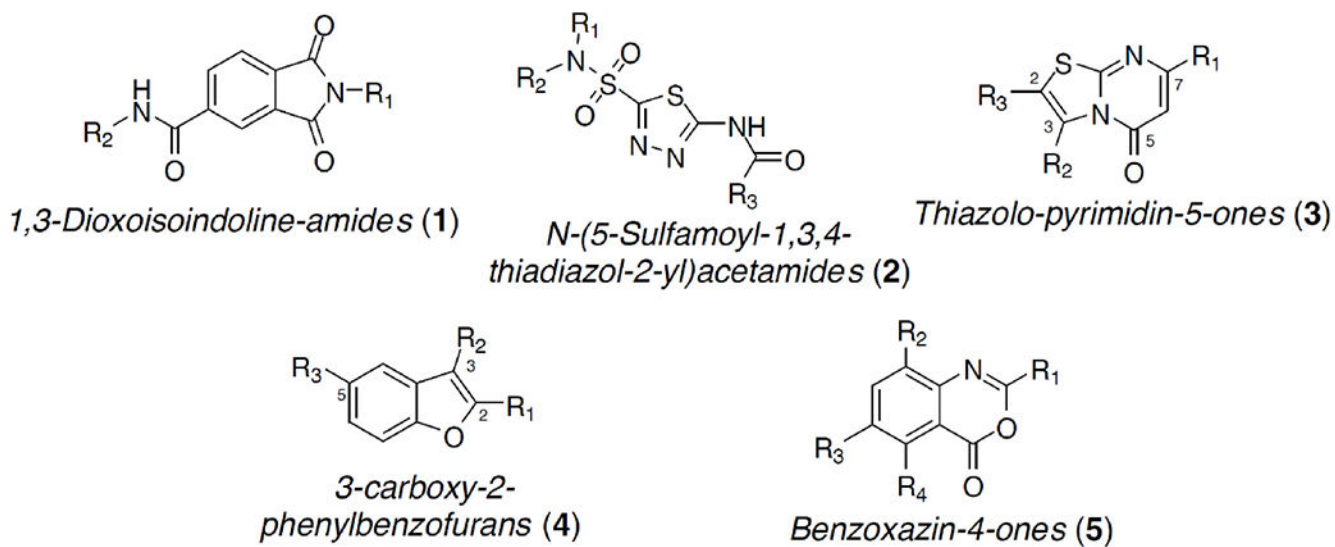
Fig. 1. Novel chemical classes of SLC26A3 inhibitors identified by high-throughput screening.
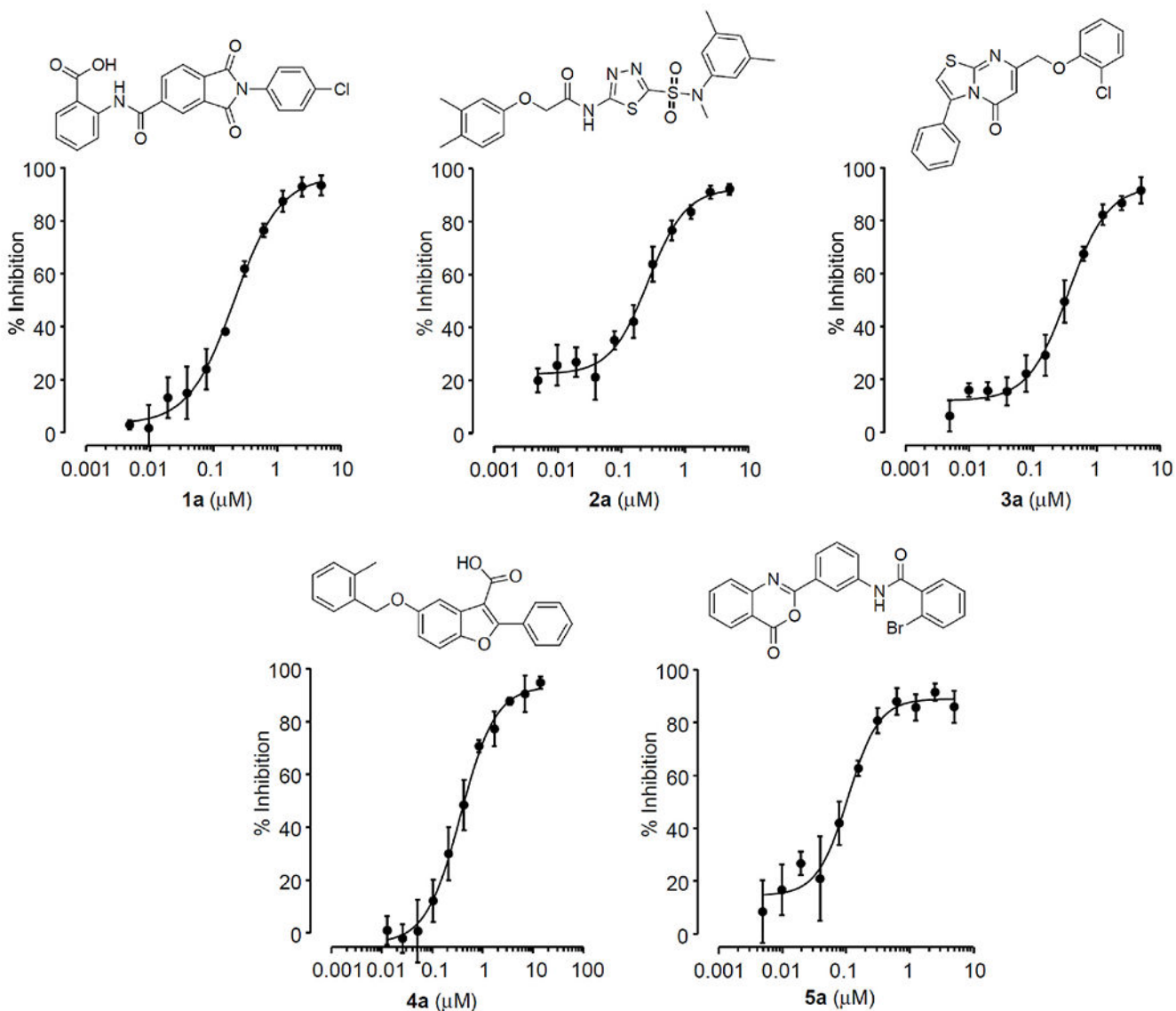Core structures shown for each of the five inhibitor classes.

Fig. 2. SLC26A3 inhibition measurements.
Structures of the most potent inhibitor from each chemical class and concentration-inhibition curves for SLC26A3 inhibition. Mean ± S.E.M., n = 3–4 experiments per compound.
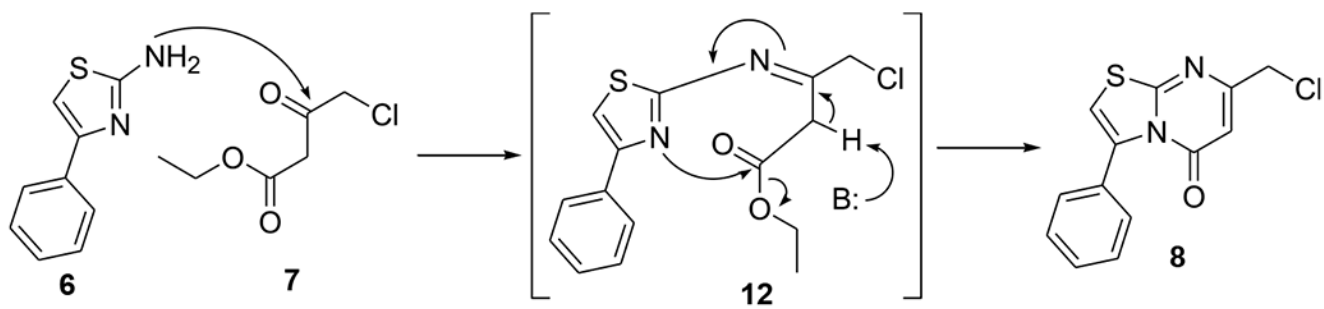
Fig. 3.
Proposed mechanism for cyclo-condensation reaction of **6** and **7** to form chloromethyl thiazolo-pyrimidin-5-one **8**.
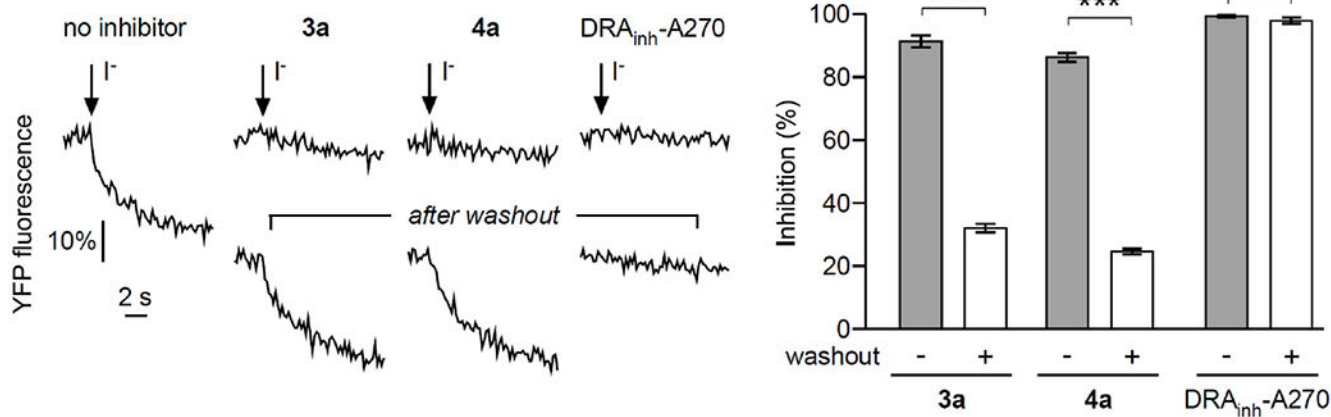
Fig. 4. Extracellular site of action of 3a and 4a.
Representative original fluorescence curves and summary data showing rapid washout of inhibitor effect for **3a** and **4a**, and slow washout for DRA_{inh}-A270. Mean ± S.E.M., n = 4 experiments per compound, Student's t-test, ***$p < 0.0001$, ns: not significant.
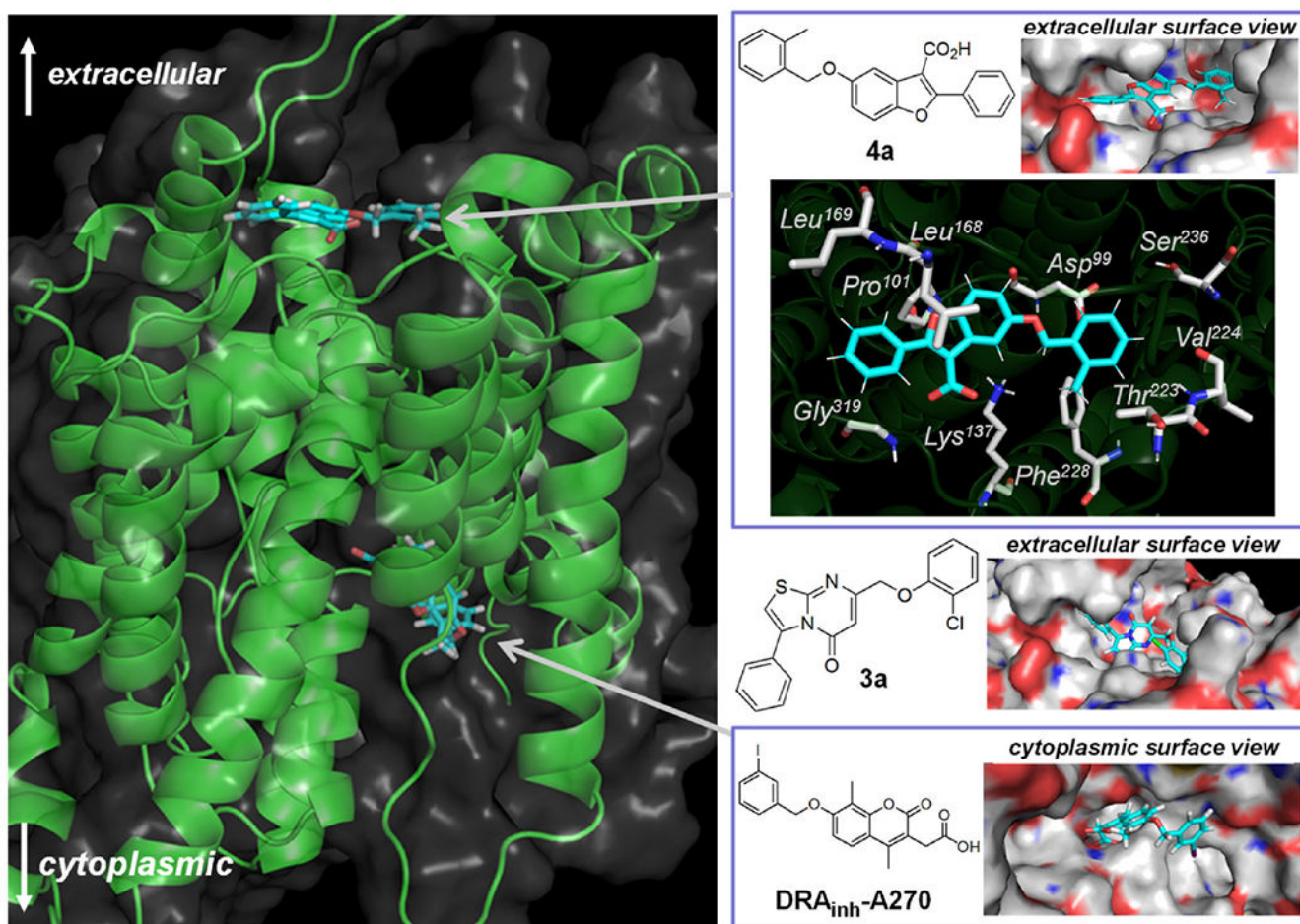
Fig. 5. Computational modeling inhibitor binding to SLC26A3.
Left. Homology model of human SLC26A3 based on mouse SLC26A9 (pdb, 6RTC) as template, and proposed inhibitor binding sites. Right. Surface representations of SLC26A3 that accommodate inhibitors in the extracellular (**4a** and **3a**), and cytoplasmic (DRA$_{inh}$-A270) domains. Specific residues that surround **4a** are indicated.
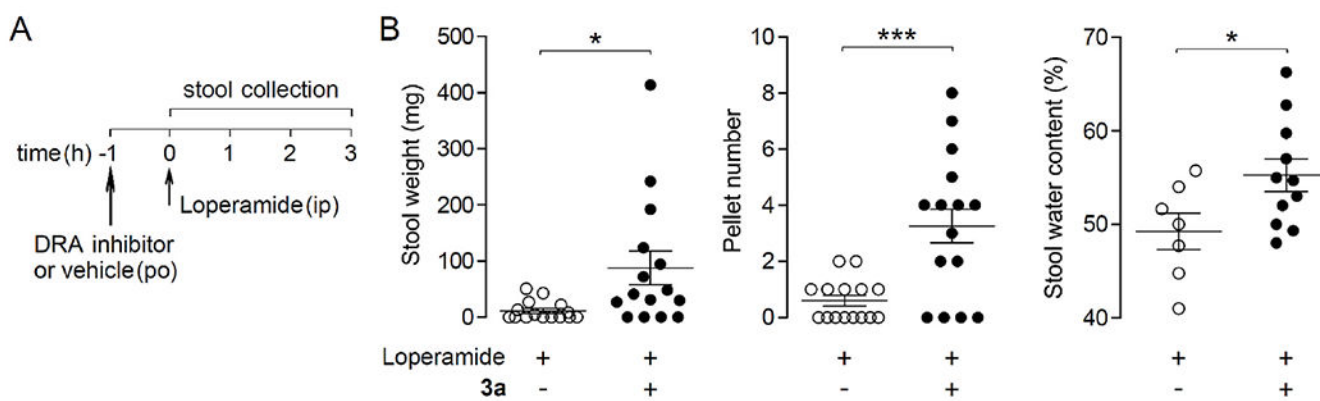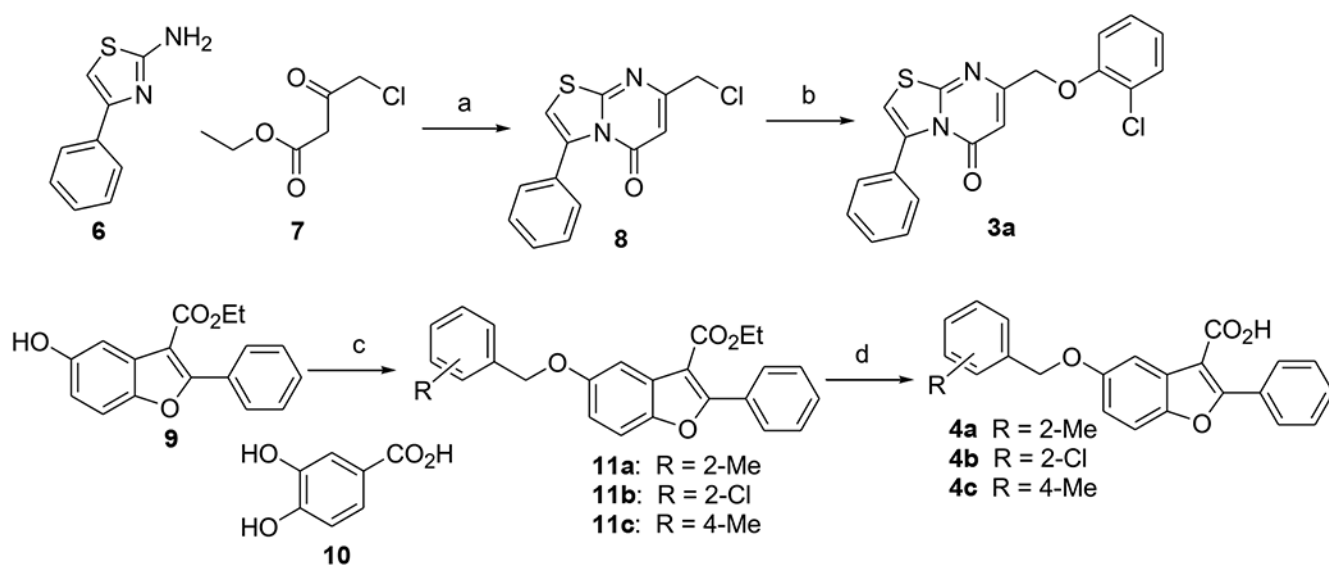
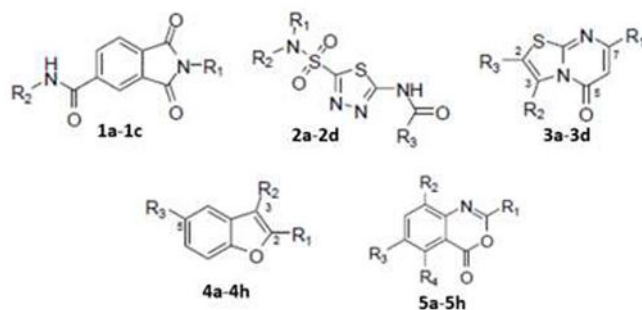**Fig. 6. Efficacy of 3a in a loperamide-induced constipation model in mice.**
A. Experimental protocol. **B.** Stool weight, number of pellets and stool water content in loperamide-treated (0.3 mg/kg, intraperitoneal) mice with and without **3a** (10 mg/kg, oral gavage). Mean ± S.E.M., 15 mice per group, Student's t-test, *p < 0.05, ***p < 0.001.

Scheme 1.
Synthesis of the most potent thiazolo-pyrimidin-5-one and 3-carboxy-2-phenylbenzofuran inhibitors. *Reagents and conditions*: (a) polyphosphoric acid (20 eq), 100 °C, 3 h; (b) 2-chlorophenol (1.0 eq), Cs_2CO_3 (1.5 eq), NaI (1.5 eq), DMF, 100 °C, 3 h; (c) substituted benzyl bromide (1.5 eq), Cs_2CO_3 (2.0 eq), 100 °C, DMF, then 3,4-dihydroxybenzoic acid (0.5 eq) scavenger (**10**), then chromatographic purification; (d) KOH (5–20 eq), THF:EtOH (1:1), 90 °C, 90 min.

Table-1

IC$_{50}$ values for the most potent SLC26A3 inhibitors from each chemical class.

Compound	R^1	R^2	R^3	IC$_{50}$ (nM)
1,3-Dioxoisoindoline-amides (1a-1c)				
1a	4-chlorophenyl	2-carboxyphenyl	–	210
1b	3,4-dimethylphenyl	2-carboxyphenyl	–	310
1c	1-isobutyl	2-carboxyphenyl	–	690
N-(5-sulfamoyl-1,3,4-thiadiazol-2-yl) acetamides (2a-2d)				
2a	3,5-dimethyl-phenyl	methyl	3,4-dimethylphenoxy-methylene	260
2b	3-methyl-phenyl	H	3-methylphenyl	470
2c	3-methyl-phenyl	H	3-methoxyphenyl	310
2d	indolin-1-yl	indolin-1-yl	4-methyl phenoxymethylene	2600
Thiazolo-pyrimidin-5-ones (3a-3d)				
3a	(2-Cl-phenoxy)-methylene	phenyl	H	360
3b	(4-Cl-benzyl)-thiomethylene	phenyl	H	540
3c	(2,4-Cl-phenoxy)-methylene	phenyl	H	1300
3d	(2-methylbenzoate)-methyl	phenyl	H	2300
3-Carboxy-2-phenyl-benzofurans (4a-4h)				
4a	phenyl	carboxylate	(2-methylbenzyl)-oxy-	340
4b	phenyl	carboxylate	(2-chlorobenzyl)-oxy-	690
4c	phenyl	carboxylate	(4-methylbenzyl)-oxy-	4000
4d	phenyl	carboxylate	(3-chlorobenzyl)-oxy-	1200
4e	phenyl	carboxylate	(4-chlorobenzyl)-oxy-	1700
4f	phenyl	carboxylate	(3,4-chlorobenzyl)oxy-	2300
4g	phenyl	carboxylate	benzyloxy	2600
4h	methyl	carboxylate methyl ester	benzyloxy-acetoxy	9800
1-Benzoxazine-4-ones (5a-5h)				
5a	*N*-(4-chlorobenzoyl)-3-aminophenyl	H	R^3 = R^4 = H	100
5b	N-(4-ethoxybenzoyl)-3-aminophenyl	H	R^3 = R^4 = H	140
5c	*N*-(2-bromobenzoyl)-3-aminophenyl	H	R^3 = R^4 = H	260
5d	*N*-(2-methoxyphenoxyacetyl)-3-aminophenyl	H	R^3 = R^4 = H	580
5e	*N*-(2,6-dimethylphenoxyacetyl)-3-aminophenyl	H	R^3 = R^4 = H	740
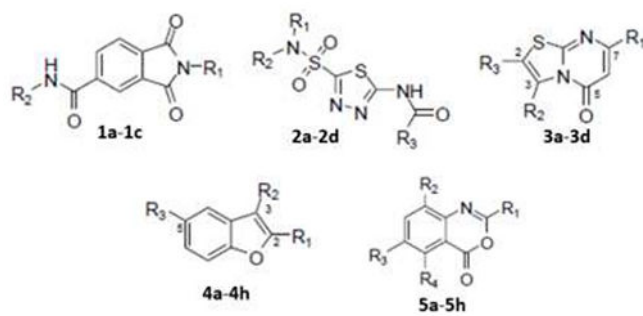
Compound	R¹	R²	R³	IC₅₀ (nM)
5f	*N*-acetyl-3-aminophenyl	H	$R^3 = R^4 = H$	740
5g	*N*-pivaloyl-3-aminophenyl	H	$R^3 = R^4 = H$	750
5h	*N*-isobutyryl-4-aminophenyl	H	$R^3 = R^4 = H$	980

Table-2

Selectivity of the most potent SLC26A3 inhibitors from each chemical class, at 10 μM concentration, against indicated ion transporters and channels. Percentage inhibition shown as mean ± S.E.M., n = 6–8 experiments per compound, per transporter. Each compound produced >90% SLC26A3 inhibition at 10 μM as shown in Fig. 2.

Compound	% Inhibition				
	SLC26A4	SLC26A6	SLC26A9	CFTR	TMEM16A
1a	−14 ± 19	35 ± 2	−4 ± 2	20 ± 0.1	0 ± 2
2a	17 ± 13	32 ± 1	−2 ± 5	5 ± 0.1	83 ± 5
3a	−13 ± 23	9 ± 2	22 ± 3	4 ± 0.1	4 ± 2
4a	−13 ± 21	37 ± 3	−8 ± 3	12 ± 0.1	2 ± 2
5a	−3 ± 13	4 ± 5	−2 ± 4	−2 ± 0.1	−1 ± 1